Electronic Supplementary Material

Facile engineering of CoS/rGO heterostructures on carbon cloth for efficient all-pH hydrogen evolution reaction and alkaline water electrolysis

Yuxian Chen,[a] *Jiayi Rong,*[a] *Qiaolin Fan,*[a] *Meng Sun,*[a] *Qiuyi Deng,*[a] *Zhonghua Ni,*[a] *Xiao Li,*[a]* *Tao Hu,*[a]*

[a] School of Mechanical Engineering, Jiangsu Key Laboratory for Design and Manufacture of Micro-Nano Biomedical Instruments, Southeast University, Nanjing, Jiangsu Province, China, 211189

Corresponding Author

*E-mail: hutao@seu.edu.cn (Tao Hu), lx2016@seu.edu.cn (Xiao Li)

This file contains:

1. Supporting figures: Figure S1~S17

2. Supporting table: Table S1~S10

1. Supporting figures: Figure S1~S12

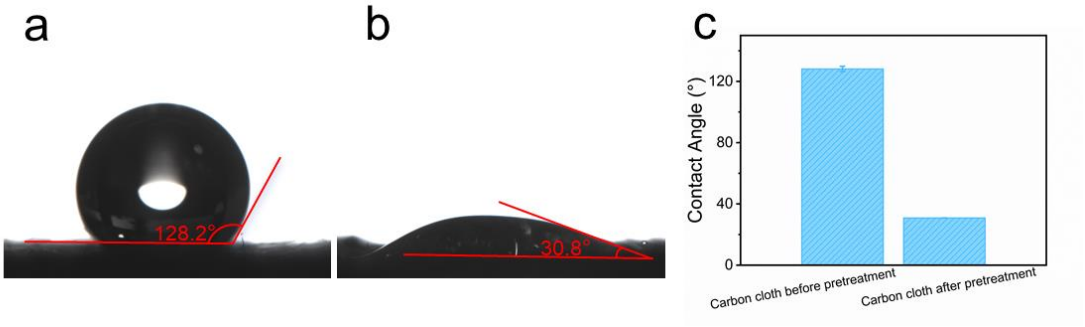

Figure S1. Contact angle measurements of carbon cloth before and after pretreatment. (a) Contact angle of pure CC before pretreatment. (b) Contact angle of pure CC after pretreatment. (c) Comparison of contact angles of carbon cloth before and after pretreatment.

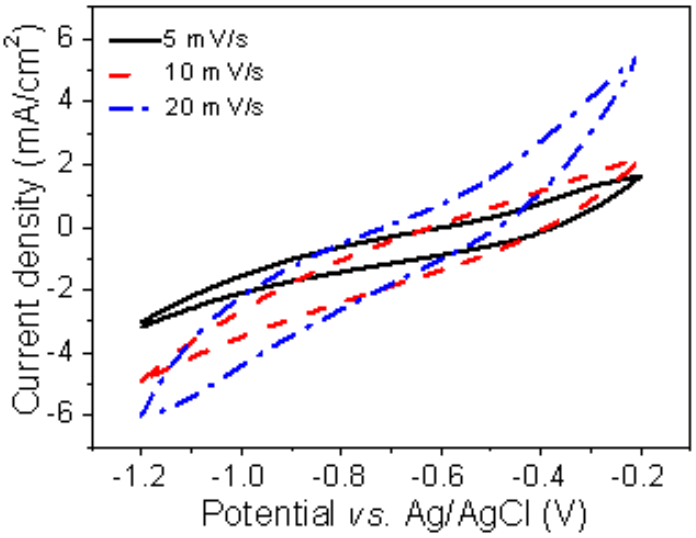

Figure S2. Cyclic voltammetric deposition curves of CoS at different scanning rates.

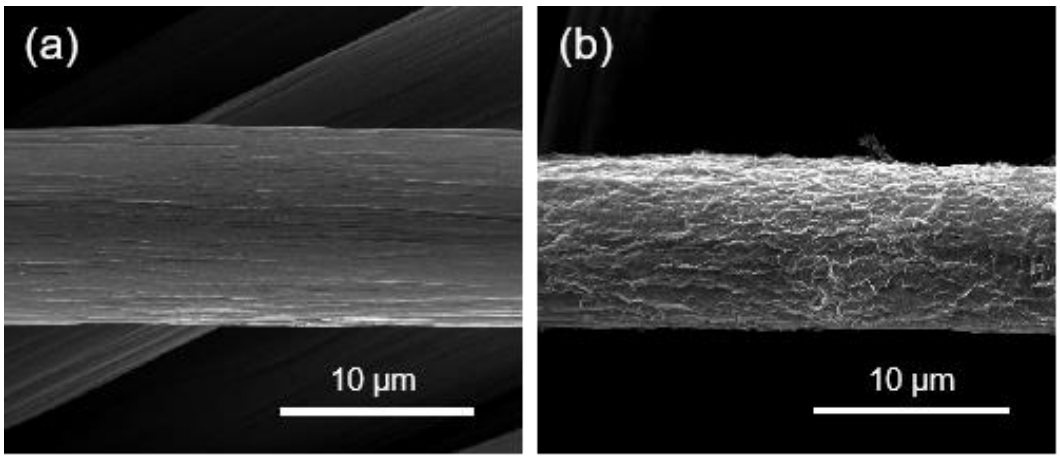

Figure S3. (a) SEM images for the carbon cloth (CC); (b) SEM images for the graphene oxide /carbon cloth (rGO@CC).

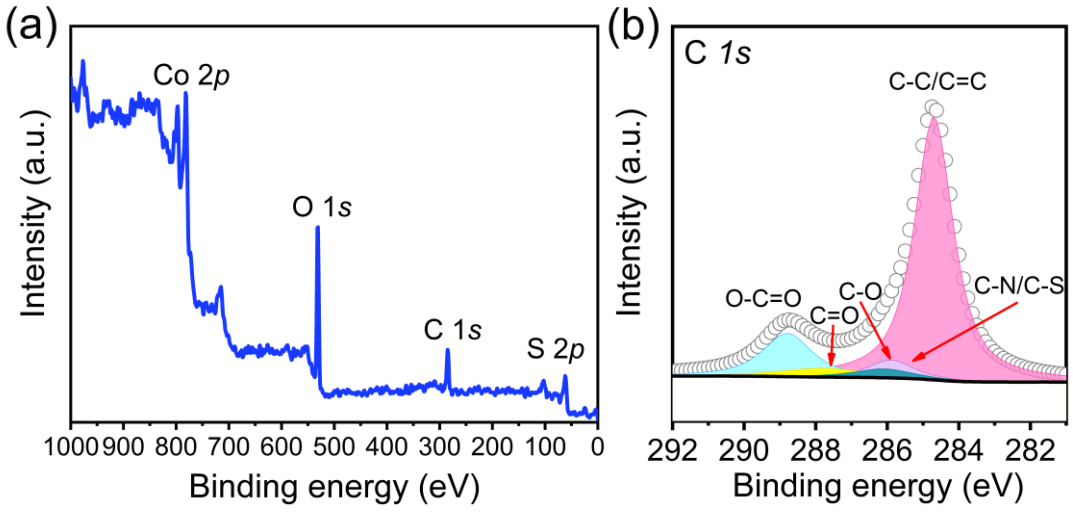

Figure S4. (a) XPS survey spectrum of CoS/rGO@CC verifies the presence of Co, O, C and S components in the material. High-resolution (b) C 1s spectra disclose the detailed chemical valences for C element.

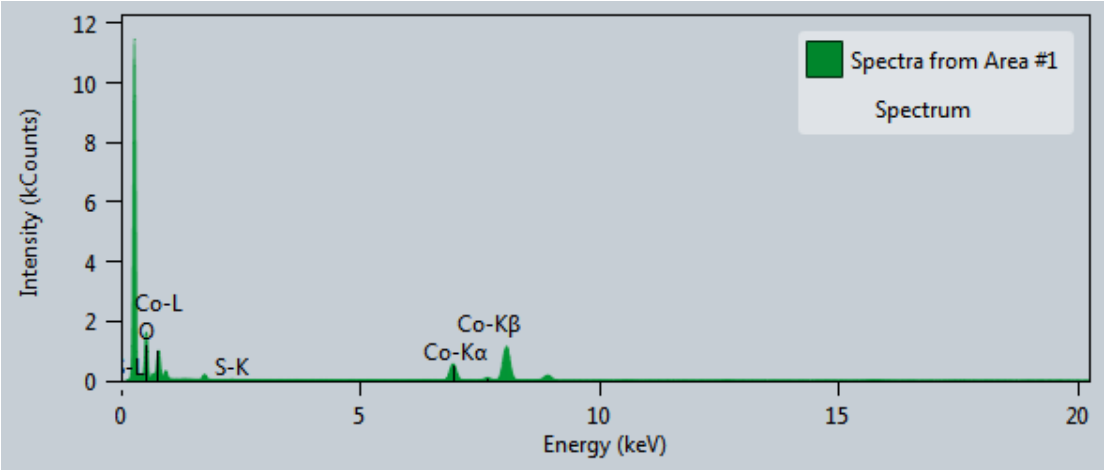

Figure S5. The EDX spectrum of CoS nanosheets on the copper mesh revealed the presence of both Co and S components in the composite material, indicating the successful synthesis of CoS.

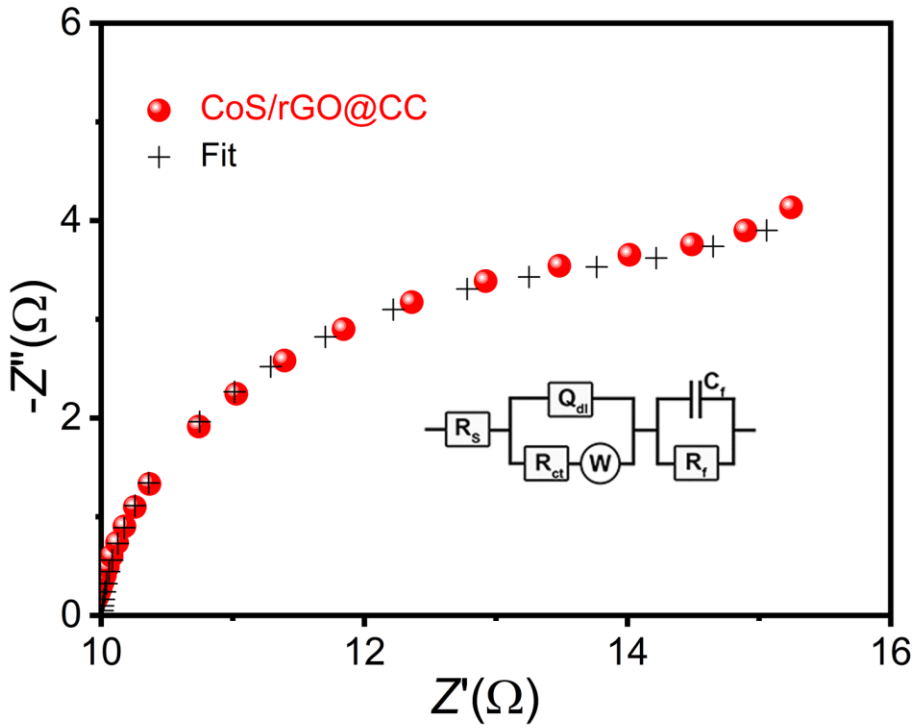

Figure S6. Nyquist plots of EIS and the corresponding fitting curve for the CoS/rGO@CC electrode, demonstrating excellent agreement between the fitting results and experimental data. The inset displays the equivalent circuit diagram.

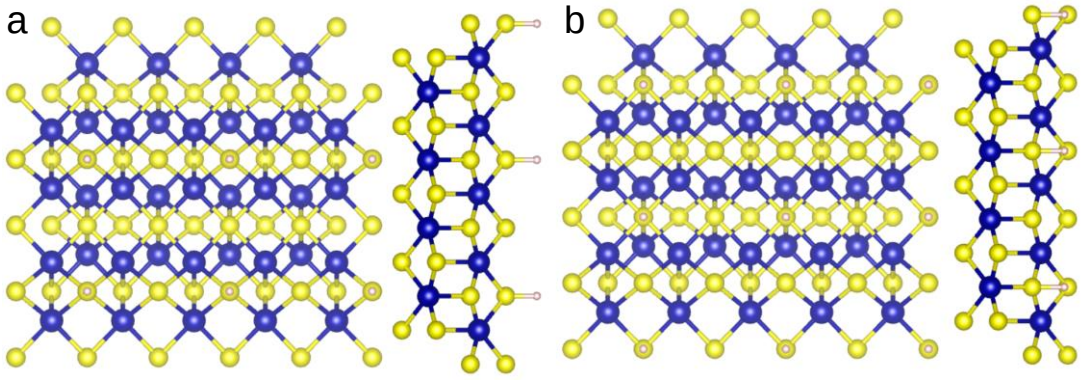

Figure S7. HER (S site adsorption) structure of pure CoS.

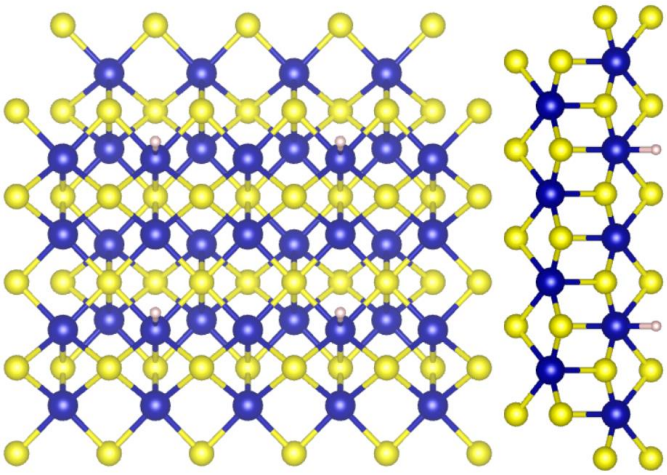

Figure S8. HER (Co site adsorption) structure of pure CoS, (a) top view (left) and (b) side view (right).

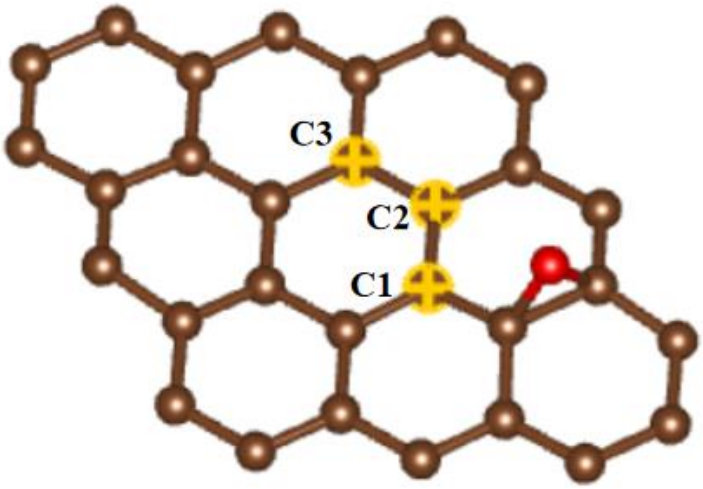

Figure S9. rGO sites in DFT calculations.

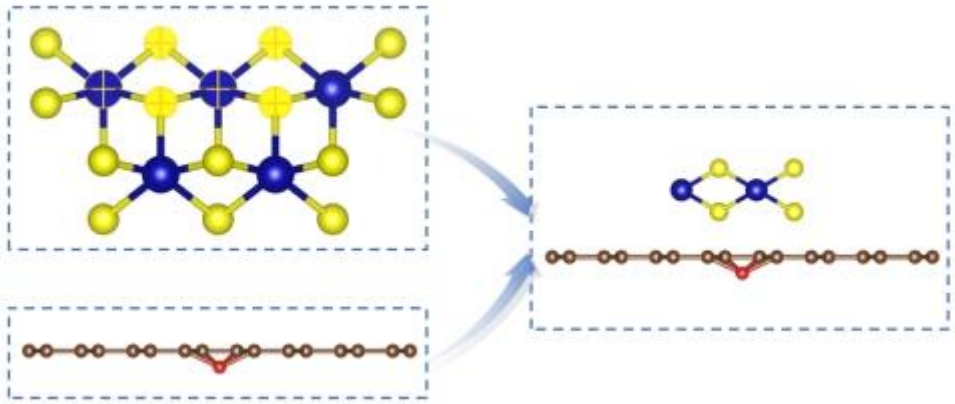

Figure S10. Design idea of DFT computational modeling.

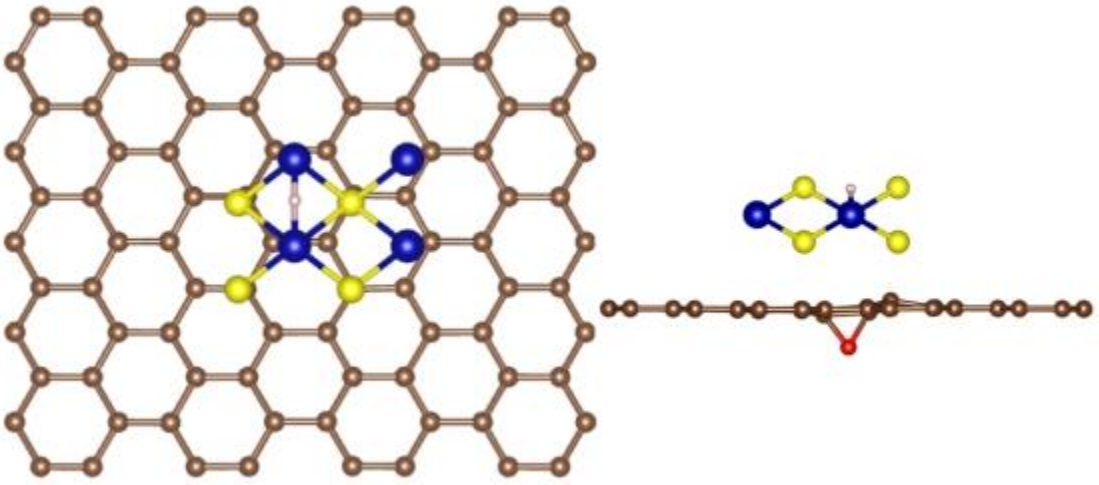

Figure S11. HER structure of CoS/rGO combined model, (a) top view (left) and (b) side view (right).

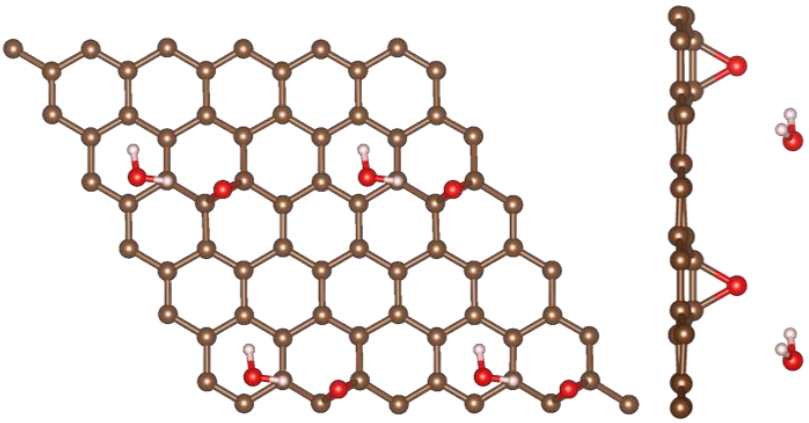

Figure S12. Water ion adsorption configuration of pure rGO during the HER process, (a) top view (left) and (b) side view (right).

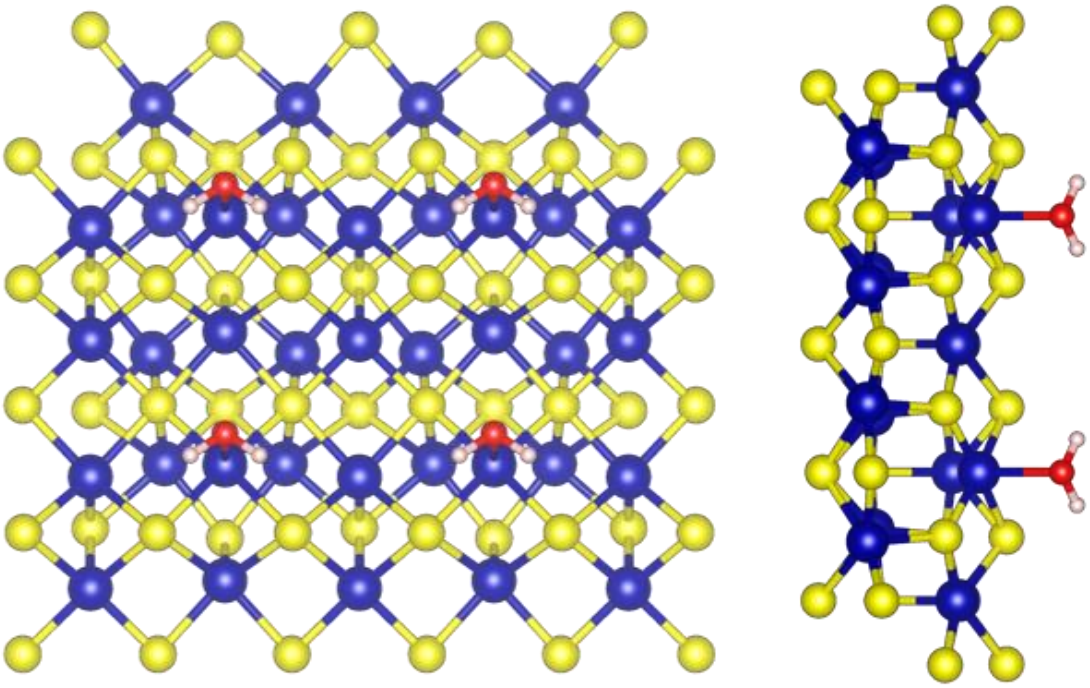

Figure S13. Water ion adsorption configuration of pure CoS during the HER process, (a) top view (left) and (b) side view (right).

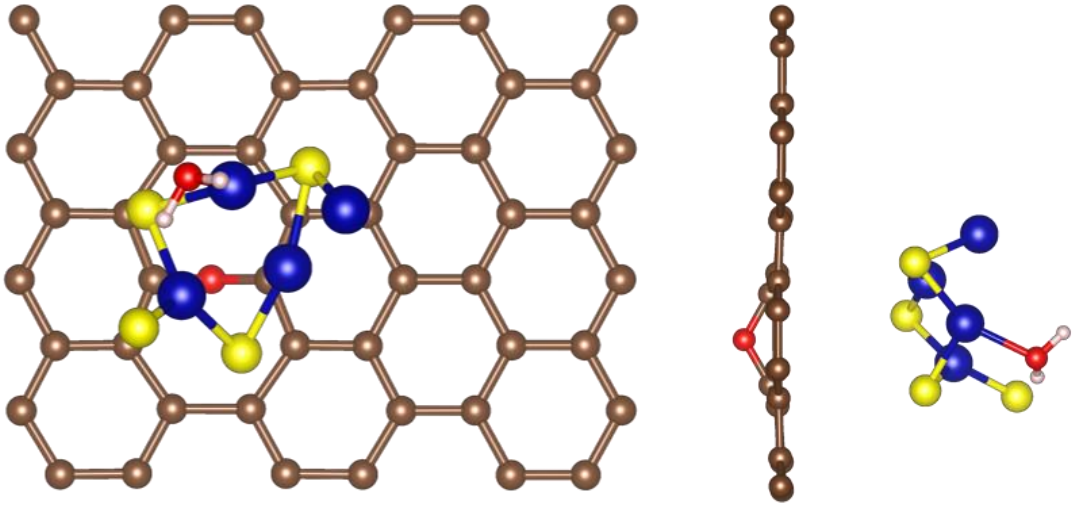

Figure S14. Water ion adsorption configuration of CoS/rGO during the HER process, (a) top view (left) and (b) side view (right).

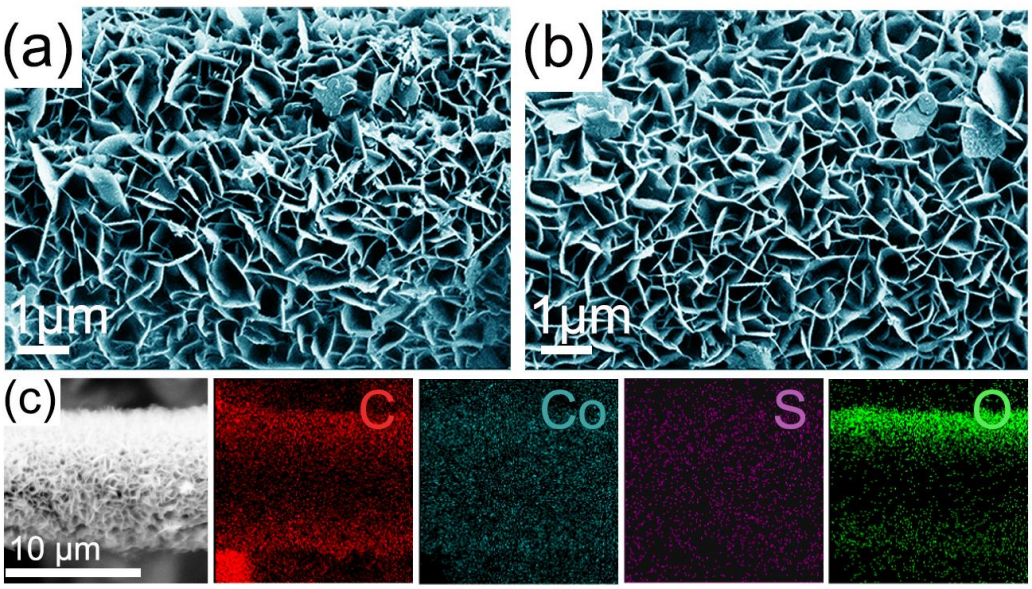

Figure S15. (a-b) presents SEM images of CoS/rGO@CC after stability test, while (c) displays elemental mappings of C, Co, S, and O.

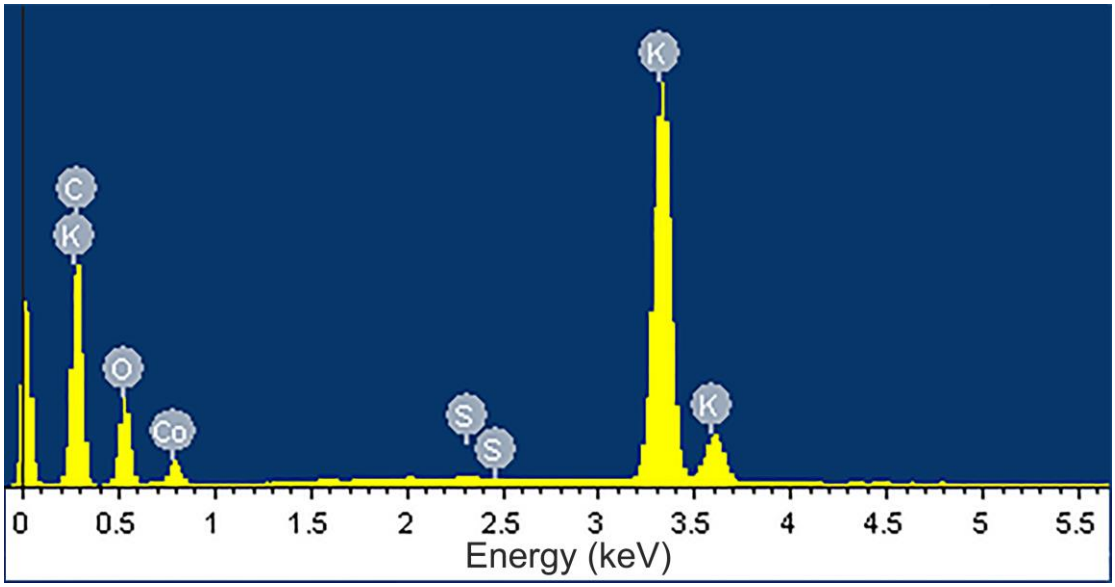

Figure S16. The EDX spectrum of CoS/rGO@CC after stability test.

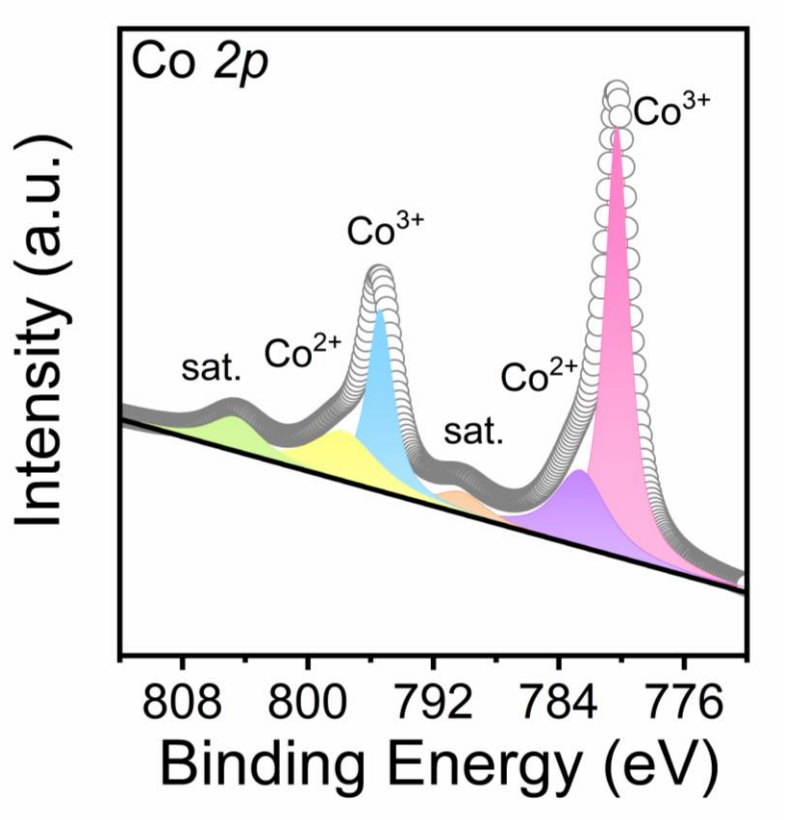

Figure S17. High-resolution Co 2p XPS spectra of CoS/rGO@CC after the OER reaction.

2. Supporting tables: Table S1~S10

Table S1. Comparison of HER activity of CoS/rGO@CC catalyst with other reference electrodes in 1 M KOH.

Electrolyte	Electrode	Onset potential (mV)	Potential at 10 mA cm^{-2}(mV)	Potential at 50 mA cm^{-2}(mV)	Tafel slope (mV dec^{-1})
1 M KOH	20% Pt/C	6.3	47.3	169.3	31.2
	CoS/rGO@CC	6.3	76.3	226.3	69
	CoS@CC	230.3	441.3	707.3	194
	rGO@CC	296.3	573.3	815.3	237

Table S2. Comparison of the HER performance of CoS/rGO@CC catalyst with recent state-of-the-art cobalt-based catalysts in KOH.

Electrolyte	Catalyst	η_{10} (mV)	Tafel slope (mV dec^{-1})	Stability time	Reference
1 M KOH	CoS/rGO@CC	76.3	69	24	This work
	CoSe/Ti	121	84	27 h	[1]
	$CoS_2/MoS_2/NC_{-25\%}$	215	80	N.A.	[2]
	PNC/Co	298	131	10 h	[3]
	Co_4S_3-NSC	352.3	150.6	N.A.	[4]
	Co-2-Ni-0.5-NC	359	373.6	N.A.	[5]
	Co-NRCNTs	370	N.A.	10 h	[6]
	Co/NGC	392	145	N.A.	[7]

Table S3. Comparison of OER activity of CoS/rGO@CC catalyst with other reference electrodes in 1 M KOH.

Electrolyte	Electrode	Onset potential (mV)	Potential at 10 mA cm^{-2} (mV)	Potential at 50 mA cm^{-2} (mV)	Tafel slope (mV dec^{-1})
1 KOH	RuO_2 on CC	325.4	400.4	543.4	106.7
	CoS/rGO@CC	232.4	290.4	398.4	71
	CoS@CC	364.4	525.4	794.4	254
	rGO@CC	406.4	605.4	>1000	332

Table S4. Comparison of the OER performance of CoS/rGO@CC catalyst with recent state-of-the-art cobalt-based catalysts in 1 M KOH.

Electrolyte	Catalyst	η10 (mV)	Tafel slope (mV dec^{-1})	Stability time	Reference
1 M KOH	CoS/rGO@CC	290.4	71	24 h	This work
	$CoSe_2$@C–CNT	310	69	N. A.	[8]
	$CoSe_2$@NC	246.7	72.66	132	[9]
	Co-N_x|P-GC/FEG	320	54	10 h	[10]
	P-CoS_2-HNA/CC	250	90	24 h	[11]
	EG/Ni_3Se_2/Co_9S_8	390	131	10 h	[12]
	EG/H-$Co_{0.85}$Se|P	410	76	10 h	[13]
	$CoSe_2$@VG/CC	418	74	25 h	[14]
	NiO/Co_3O_4	240	73	48 h	[15]

Table S5. The charge-transfer resistance (Rct) of different electrodes.

Electrode	Rct	
	Value (Ω)	Error (%)
20% Pt/C	3423	2.034
RuO_2 on CC	7.2357	0.649
CoS/rGO@CC	6.3	6.955
CoS@CC	374.41	0.792
rGO@CC	103.54	0.895
CC	1365	0.684

Table S6. Comparison of overall water splitting voltages with various recently reported catalysts.

Electrolyte	Catalyst	Voltage (mV)	Reference
1 M KOH	CoS/rGO@CC||CoS/rGO@CC	744	This work
	CoS/rGO@CC||20% Pt/C	925	This work
	CoS/rGO@CC||RuO_2 on CC	1005	This work
	RuO_2@Co_3O_4(1:6)||RuO_2@Co_3O_4(1:6)	1460	[16]
	DH-CuCo-P @ NC/CC||DH-CuCo-P @ NC/CC	1494	[17]
	1T′/1T Co,P-SnS_2||1T′/1T Co,P-SnS_2	1530	[18]
	CoMoP@Co_3O_{4-x}||CoMoP@Co_3O_{4-x}	1614	[19]
	Co_3O_4–Mo_2N NFs||Co_3O_4–Mo_2N NFs	1650	[20]
	VOB-Co_3O_4/NF||VOB-Co_3O_4/NF	1670	[21]
	$Co_6Mo_6C_2$/$Co_2Mo_3O_8$||$Co_6Mo_6C_2$/$Co_2Mo_3O_8$	1810	[22]

Table S7. Comparison of HER activity of CoS/rGO@CC catalyst with other reference electrodes in 0.5 M H_2SO_4.

Electrolyte	Electrode	Onset potential (mV)	Potential at 10 mA cm^{-2}(mV)	Potential at 50 mA cm^{-2}(mV)	Tafel slope (mV dec^{-1})
0.5 M H_2SO_4	20% Pt/C	15.4	31.4	82.4	34.1
	CoS/rGO@CC	12.4	41.4	121.4	45.2
	CoS@CC	45.4	113.4	363.4	112
	rGO@CC	53.4	132.4	412.4	135.4

Table S8. Comparison of the HER performance of CoS/rGO@CC catalyst with recent state-of-the-art cobalt-based catalysts in 0.5 M H_2SO_4.

Electrolyte	Catalyst	η_{10} (mV)	Tafel slope (mV dec^{-1})	Stability time	Reference
0.5 M H_2SO_4	CoS/rGO@CC	41	45	24	This work
	Co–P@PC-750	72	49	20 h	[23]
	Fe/P-CoS2	80	56	10 h	[24]
	CoP NFs	122	54.8	N. A.	[25]
	CoP/Ni2P@HPNCP	130	64.91	30 h	[25]
	Fe–CoSe2@NC	143	40.9	48 h	[26]
	CoP/CN@ MoS2	144	69	N. A.	[27]
	Sn-CoS2/CC	161	94	32 h	[28]
	Co-NRCNTs	260	69	8.5 h	[6]

Table S9. Comparison of HER activity of CoS/rGO@CC catalyst with other reference electrodes in 1 M PBS.

Electrolyte	Electrode	Onset potential (mV)	Potential at 10 mA cm^{-2}(mV)	Potential at 50 mA cm^{-2}(mV)	Tafel slope (mV dec^{-1})
1 M PBS	20% Pt/C	95.7	302.7	482.7	168.8
	CoS/rGO @CC	87.7	315.7	549.7	201.99
	CoS@CC	124.7	367.7	710.7	243.05
	rGO@CC	122.7	610.7	>1000	379.2

Table S10. In neutral media, the HER performance of the CoS-rGO@CC catalyst is compared with that of recent advanced catalysts.

Electrolyte	Catalyst	η10 (mV)	Tafel slope (mV dec^{-1})	Stability time	Reference
Natural Media	CoS/rGO@CC	315	202	22	This work
	$CoO/CoSe_2$	337	131	9 h	[29]
	FeP NPs@NPC	433	149	10 h	[30]
	FeP/NCNSs	409	92	10 h	[31]
	HF-MoSP-800	456	N. A.	N. A.	[32]
	Fe@N-CNT/IF	525	199.6	12 h	[33]
	NiSx film	576	123	N. A.	[34]
	CuS nanoparticles	584	316	14 h	[35]

References

[1] T. Liu, Q. Liu, A.M. Asiri, et al., An amorphous CoSe film behaves as an active and stable full water-splitting electrocatalyst under strongly alkaline conditions, Chem. Commun. 51 (2015) 16683-16686.

[2] K. Ji, K. Matras-Postolek, R. Shi, et al., MoS_2/CoS_2 heterostructures embedded in N-doped carbon nanosheets towards enhanced hydrogen evolution reaction, J. Alloys Compd. 891 (2022) 161962.

[3] X. Li, Z. Niu, J. Jiang, et al., Cobalt nanoparticles embedded in porous N-rich carbon as an efficient bifunctional electrocatalyst for water splitting, J. Mater. Chem. A 4 (2016) 3204-3209.

[4] Y. Liu, X. Luo, C. Zhou, et al., A modulated electronic state strategy designed to integrate active HER and OER components as hybrid heterostructures for efficient overall water splitting, Appl. Catal. B: Environ. 260 (2020) 118197.

[5] X. Shen, W. Tan, Z. Wei, et al., Co-modified Ni/N-doped carbon as electrocatalysts for HER and OER, J. Mater. Sci.: Mater. Electron. 32 (2021) 22974-22983.

[6] X. Zou, X. Huang, A. Goswami, et al., Cobalt-Embedded Nitrogen-Rich Carbon Nanotubes Efficiently Catalyze Hydrogen Evolution Reaction at All pH Values, Angew. Chem. Int. Ed. 53 (2014) 4372-4376.

[7] J. Li, Y. Kang, D. Liu, et al., Nitrogen-Doped Graphitic Carbon-Supported Ultrafine Co Nanoparticles as an Efficient Multifunctional Electrocatalyst for HER and Rechargeable Zn-Air Batteries, ACS Appl. Mater. Inter. 12 (2020) 5717-5729.

[8] M. Yuan, M. Wang, P. Lu, et al., Tuning carbon nanotube-grafted core-shell-structured cobalt selenide@carbon hybrids for efficient oxygen evolution reaction, J. Colloid Interface Sci. 533 (2019) 503-512.

[9] J. Lu, S. Wang, C. Ding, et al., Metal organic frameworks derived CoSe2@N-Doped-carbon-nanorods as highly efficient electrocatalysts for oxygen evolution reaction, J. Alloys Compd. 778 (2019) 134-140.

[10] Y. Hou, M. Qiu, T. Zhang, et al., Efficient Electrochemical and Photoelectrochemical Water Splitting by a 3D Nanostructured Carbon Supported on Flexible Exfoliated Graphene Foil, Adv. Mater. 29 (2017) 1604480.

[11] Y. Li, Z. Mao, Q. Wang, et al., Hollow nanosheet array of phosphorus-anion-decorated cobalt disulfide as an efficient electrocatalyst for overall water splitting, Chem. Eng. J. 390 (2020) 124556.

[12] Y. Hou, M. Qiu, G. Nam, et al., Integrated Hierarchical Cobalt Sulfide/Nickel Selenide Hybrid Nanosheets as an Efficient Three-dimensional Electrode for Electrochemical and Photoelectrochemical Water Splitting, Nano Lett. 17 (2017) 4202-4209.

[13] Y. Hou, M. Qiu, T. Zhang, et al., Ternary Porous Cobalt Phosphoselenide Nanosheets: An Efficient Electrocatalyst for Electrocatalytic and Photoelectrochemical Water Splitting, Adv. Mater. 29(35) (2017) 1701589.

[14] Z. Xia, H. Sun, X. He, et al., In situ construction of $CoSe_2$@vertical-oriented graphene arrays as self-supporting electrodes for sodium-ion capacitors and electrocatalytic oxygen evolution, Nano Energy. 60 (2019) 385-393.

[15] M. Tahir, L. Pan, R. Zhang, et al., High-Valence-State NiO/Co_3O_4 Nanoparticles on Nitrogen-Doped Carbon for Oxygen Evolution at Low Overpotential, ACS Energy Lett. 2 (2017) 2177-2182.

[16] Y. Jiang, H. Liu, Y. Jiang, et al., Adjustable heterointerface-vacancy enhancement effect in RuO_2@Co_3O_4 electrocatalysts for efficient overall water splitting, Appl. Catal. B: Environ. 324 (2023) 122294.

[17] B.C. Lund, T.E. Abrams, A.A. Gravely, Rebuttal to Gravely et al. Validity of PTSD diagnoses in VA administrative data: comparison of VA administrative PTSD diagnoses to self-reported PTSD Checklist scores, J. Rehabil. Res. Dev. 48(1) (2011) 21-30.

[18] M. Singh, T.T. Nguyen, P.M.A., et al., Metallic Metastable Hybrid 1T'/1T Phase Triggered Co,P-SnS_2 Nanosheets for High Efficiency Trifunctional Electrocatalyst, Small. 19 (2023) e2206726.

[19] Y. Hao, G. Du, Y. Fan, et al., Mo/P Dual-Doped Co/Oxygen-Deficient Co_3O_4 Core-Shell Nanorods Supported on Ni Foam for Electrochemical Overall Water Splitting, ACS Appl. Mater. Inter. 13 (2021) 55263-55271.

[20] T. Wang, P. Wang, W. Zang, et al., Nanoframes of Co_3O_4–Mo_2N Heterointerfaces Enable High-Performance Bifunctionality toward Both Electrocatalytic HER and OER, Adv. Funct. Mater. 32(7) (2021) 2107382.

[21] H. Yuan, S. Wang, Z. Ma, et al., Oxygen vacancies engineered self-supported B doped Co_3O_4 nanowires as an efficient multifunctional catalyst for electrochemical water splitting and hydrolysis of sodium borohydride, Chem. Eng. J. 404 (2021) 126474.

[22] R. Liu, M. Anjass, S. Greiner, et al., Bottom-up Design of Bimetallic Cobalt-Molybdenum Carbides/Oxides for Overall Water Splitting, Chemistry. 26 (2020) 4157-4164.

[23] J. Wu, D. Wang, S. Wan, et al., An efficient cobalt phosphide electrocatalyst derived from cobalt phosphonate complex for all-pH hydrogen evolution reaction and overall water splitting in alkaline solution, Small. 16(15) (2020) 1900550.

[24] Y.Y. Zhang, X. Zhang, Z.Y. Wu, et al., Fe/P dual doping boosts the activity and durability of CoS_2 polycrystalline nanowires for hydrogen evolution, J. Mater. Chem. A. 7 (2019) 5195-5200.

[25] L. Ji, J. Wang, X. Teng, et al., CoP Nanoframes as Bifunctional Electrocatalysts for Efficient Overall Water Splitting, ACS Catal. 10 (2019) 412-419.

[26] X. Wu, S. Han, D. He, et al., Metal Organic Framework Derived Fe-Doped $CoSe_2$ Incorporated in Nitrogen-Doped Carbon Hybrid for Efficient Hydrogen Evolution, ACS Sustain. Chem. Eng. 6 (2018) 8672-8678.

[27] J. G. Li, K. Xie, H. Sun, et al., Template-directed bifunctional dodecahedral CoP/CN@MoS_2 electrocatalyst for high efficient water splitting, ACS Appl. Mater. Inter. 11 (2019) 36649-36657.

[28] F. Liu, W. He, Y. Li, et al., Activating sulfur sites of CoS_2 electrocatalysts through tin doping for hydrogen evolution reaction, Appl. Surf. Sci. 546 (2021) 149101.

[29] T. Feng, F. Wang, J. Lei, et al., A universal CoO/$CoSe_2$ heterostructure electrocatalyst towards hydrogen evolution reaction via in-situ partial surface-oxidation-selenization method, Mater. Chem. Phys. 267 (2021) 124644.

[30] Z. Pu, I. S. Amiinu, C. Zhang, et al., Phytic acid-derivative transition metal phosphides encapsulated in N,P-codoped carbon: an efficient and durable hydrogen evolution electrocatalyst in a wide pH range, Nanoscale 9 (2017) 3555-3560.

[31] Y. Yu, Z. Peng, M. Asif, et al., FeP Nanocrystals Embedded in N-Doped Carbon Nanosheets for Efficient Electrocatalytic Hydrogen Generation over a Broad pH Range, ACS Sustain. Chem. Eng. 6 (2018) 11587-11594.

[32] A. Wu, C. Tian, H. Yan, et al., Hierarchical MoS2@MoP core–shell heterojunction electrocatalysts for efficient hydrogen evolution reaction over a broad pH range, Nanoscale 8 (2016) 11052-11059.

[33] J. Yu, G. Li, H. Liu, et al., Electrochemical flocculation integrated hydrogen evolution reaction of Fe@N-doped carbon nanotubes on iron foam for ultralow voltage electrolysis in neutral media, Adv. Sci. 6(18) (2019) 1901458.

[34] Y. Çimen, A. W. Peters, J. R. Avila, et al., Atomic layer deposition of ultrathin nickel sulfide films and preliminary assessment of their performance as hydrogen evolution catalysts, Langmuir 32 (2016) 12005-12012.

[35] M. Patel, K. K. Joshi, K. H. Modi, et al., CuS nanoparticles: an efficient electrocatalyst for hydrogen evolution reaction in a wide pH range, Electrochim. Acta 441 (2023) 141740.